Two-fluid equilibrium analysis of spherical torus plasmas sustained by multi-pulsing coaxial helicity injection

T. Kanki[1], M. Nagata[2]

[1] *Japan Coast Guard Academy, Kure, Japan*

[2] *University of Hyogo, Himeji, Japan*

Solenoid-less non-inductive current start-up and steady-state current drive techniques in the spherical torus (ST) have been studied using the coaxial helicity injection (CHI). Recently, a new approach of the CHI operated in multi-pulsing CHI (M-CHI) has been proposed [1]. The M-CHI scenario is that after the plasma current partially decays, a new CHI pulse is applied and the cycle process is repeated to achieve a quasi-steady sustainment and good confinement. To examine the dynamo current drive of ST by the M-CHI, we started the double-pulsing operations in the HIST device, observing that the steep density gradient between the central open flux column (OFC) and closed flux regions causes not only the $\boldsymbol{E}\times\boldsymbol{B}$ drift but also the ion diamagnetic drift to exhibit the two-fluid effect and Hall dynamo [2]. The purpose of this study is to investigate the effect of the M-CHI on the two-fluid equilibrium configurations of ST.

For the two-fluid equilibrium calculations, let us assume axisymmetry about HIST geometric axis in cylindrical coordinates (r, θ, z). Using the dimensionless variables, an axisymmetric two-fluid flowing equilibrium can be described by a pair of generalized Grad-Shafranov equations for the ion surface variable Y and the electron surface variable ψ [3],

$$\overline{\psi}_i' r^2 \nabla\cdot\left(\frac{\overline{\psi}_i'}{n}\frac{\nabla Y}{r^2}\right)=\frac{r}{\varepsilon}\left(B_\theta\overline{\psi}_i'-nu_\theta\right)+nr^2\left(H_i'-T_iS_i'\right), \tag{1}$$

$$r^2\nabla\cdot\left(\frac{\nabla\psi}{r^2}\right)=\frac{r}{\varepsilon}\left(B_\theta\overline{\psi}_e'-nu_\theta\right)-nr^2\left(H_e'-T_eS_e'\right), \tag{2}$$

and a generalized Bernoulli equations for the number density n,

$$\frac{\gamma}{\gamma-1}n^{\gamma-1}\exp\left[(\gamma-1)S_i\right]+\frac{u^2}{2}+\phi_E=H_i, \tag{3}$$

$$\frac{\gamma}{\gamma-1}n^{\gamma-1}\exp\left[(\gamma-1)S_e\right]-\phi_E=H_e. \tag{4}$$

Here $\boldsymbol{u}$, $\boldsymbol{B}$, T_α, ϕ_E, and γ are the ion flow velocity, magnetic field, temperature of species (α=i, e), electrostatic potential, and adiabatic constant, respectively. Also, the two-fluid parameter ε is defined by the ratio of the ion skin depth $\ell_i=\sqrt{m_i/(\mu_0 ne^2)}$ (m_i and e are the ion mass and electron charge, respectively.) to the system length scale R (the effective radius of the flux conserver (FC) used in the HIST, R=0.45 m), and ε=0.0716 is given by using $\ell_i=3.2$ cm

through $n = 5.0 \times 10^{19}$ m^{-3} observed in the HIST experiment. The value of γ is assumed as 5/3 in the calculation. Note that ψ corresponds to the familiar poloidal flux function. The poloidal flow stream function $\overline{\psi}_\alpha$, total enthalpy function H_α, and entropy function S_α are arbitrary surface functions of their respective surface variables. The three arbitrary functions $\Lambda_\alpha (\equiv \overline{\psi}_\alpha')$, H_α, and S_α for each species can be assumed so as to reflect the experimental results by choosing appropriate function forms,

$$\Lambda_\alpha(x) = \Lambda_{\alpha 0} + (\Lambda_{\alpha 1} - \Lambda_{\alpha 0}) \left. \frac{df}{dx} \right|_{x-\Delta x_\alpha ; \delta_{\alpha 0}, \delta_{\alpha 1}, \delta_{\alpha 2}}, \tag{5}$$

$$H_\alpha(x) = H_{\alpha 0} + (H_{\alpha 1} - H_{\alpha 0}) \left. \frac{dg}{dx} \right|_{x-\Delta x_{H\alpha} ; \delta_{H\alpha 1}, \delta_{H\alpha 2}}, \tag{6}$$

$$S_\alpha(x) = S_{\alpha 0} + (S_{\alpha 1} - S_{\alpha 0}) \left. \frac{dg}{dx} \right|_{x-\Delta x_{S\alpha} ; \delta_{S\alpha 1}, \delta_{S\alpha 2}}, \tag{7}$$

$$f(x;\delta_0,\delta_1,\delta_2) = \begin{cases} -\dfrac{1}{\delta_0\delta_1}\left[\dfrac{\delta_0^4}{12}\left(1-\dfrac{2\delta_1}{\delta_0}\right) + x^2\left\{\dfrac{\delta_0\delta_1}{2} + x\left(\dfrac{\delta_0+\delta_1}{3}+\dfrac{x}{4}\right)\right\}\right]; & x < 0 \\ -\dfrac{\delta_0^3}{12\delta_1}\left(1-\dfrac{2\delta_1}{\delta_0}\right) - \delta_2\left\{x - \delta_2 \log\left(1+\dfrac{x}{\delta_2}\right)\right\}; & x \geq 0 \end{cases}, \tag{8}$$

$$g(x;\delta_1,\delta_2) = \frac{1}{\delta_1+\delta_2}\begin{cases} \delta_1^2 \exp[x/\delta_1]; & x < 0 \\ \delta_1 x + \delta_2\sqrt{\delta_2^2 + x^2} - \delta_2^2 + \delta_1^2; & x \geq 0 \end{cases}. \tag{9}$$

Here $\Lambda_{\alpha 0}, \Lambda_{\alpha 1}, H_{\alpha 0}, H_{\alpha 1}, S_{\alpha 0}, S_{\alpha 1}, \Delta x_\alpha, \delta_{\alpha 0}, \delta_{\alpha 1}, \delta_{\alpha 2}, \Delta x_{H\alpha}, \delta_{H\alpha 1}, \delta_{H\alpha 2}, \Delta x_{S\alpha}, \delta_{S\alpha 1}$, and $\delta_{S\alpha 2}$ are constant parameters. To complete two-fluid equilibrium system, we need the auxiliary equations, $Y \equiv \psi + \varepsilon r u_\theta$, $B_\theta = (\overline{\psi}_i - \overline{\psi}_e)/\varepsilon r$, $u_p = |\nabla \overline{\psi}_i| / nr$, and $T_\alpha = n^{\gamma-1} \exp[(\gamma-1)S_\alpha]$. Here u_p is the ion poloidal flow velocity. Equations (1) and (2) have terms of order $1/\varepsilon$ on the right-hand side, and they cause singularities. We employ the nearby-fluids procedure to eliminate the singularities [3].

Next, we consider the boundary conditions for Eqs. (1)-(4). No magnetic flux penetrates the FC, central conductor, and entrance port of the FC. Therefore, ψ is fixed at 0 at the FC wall and surface of the central conductor and entrance port. The bias flux is given by assigning fixed values of ψ to grid points corresponding to the right open end. These values are calculated using the formula,

$$\psi_{\text{bias}}(r) = \frac{4\psi_s}{(R_e - R_c)^2}(r - R_c)(R_e - r), \tag{10}$$

where R_c and R_e are the radii of the central conductor and entrance port, and ψ_s is the maximum value of the bias flux. This Dirichlet boundary condition is used for solving Eq. (2) for ψ. The

vacuum toroidal magnetic field $B_{t.v}$ is produced by a toroidal field coil current I_{tf} along the geometric axis inside the central conductor. The boundary condition of the flow velocity is required to solve Eq. (1) for u_θ. We impose the free-slip boundary condition corresponding to no friction at the Dirichlet boundaries. Under the above assumptions and boundary conditions, the equilibrium is numerically determined by using a successive over-relaxation method for updating ψ and a Newton-Raphson method for updating n [4].

On the basis of the numerical results, we investigate the effect of the M-CHI on the two-fluid equilibria. By driving the poloidal current I_p again along the open field lines through applying a new CHI pulse (M-CHI effect), the magnetic helicity is injected again into the plasma through the linkage of the toroidal flux which links the bias poloidal flux. We consider that increasing the poloidal electron flow velocity u_{ez} along the open field lines drives the poloidal current on the open flux region. Therefore, we increase the absolute edge value of the u_{ez} by decreasing the value of Λ_{e0} related to the strength of u_{ez}. Figure 1 shows the radial profiles of u_{ez} at the midplane. Note that the cases I, II, and III correspond to Λ_{e0} =-0.15, -0.16, and -0.17, respectively. In Fig. 1, u_{ez} can be clearly seen to be decreased in the OFC region as the values of Λ_{e0} become smaller. The negative values of u_{ez} represent the opposite direction to I_p and I_{tf}. As shown in Fig. 2, the poloidal ion flow velocity u_z in the opposite direction to u_{ez}, but in the same direction as I_p is increased in the OFC region, enhancing the flow shear around the separatrix in the high magnetic field side, and contributing to the increment of I_p. This is because the ion diamagnetic drift velocity u_{dia} is changed in the same direction as the $\boldsymbol{E} \times \boldsymbol{B}$ drift velocity u_E around the separatrix through the negative ion pressure gradient as shown in Fig. 3. Here u_{dia} is comparable to u_E, but the ion inertial drift velocity is small. Due to the M-CHI effect, the shear of u_E is enhanced around the separatrix, but the direction of u_E does not change there. As shown in Fig. 4, the density n is decreased in the closed flux region and its negative gradient around the separatrix steepens. The decrease in the density related to the enthalpy, $h_\alpha = (\gamma n^{\gamma-1}/\gamma - 1)\exp[(\gamma - 1)S_\alpha]$ can be explained using the generalized Bernoulli equations that the increase in the ion flow energy causes the decrease in the enthalpy. The ion temperature profile is almost kept broad one around the separatrix in spite of the M-CHI effect. Therefore, the negative gradient of the ion pressure can be caused depending on that of the density. This steep density gradient can be observed in the HIST experiment when the CHI pulse is applied again during the partial decay of plasma current. As shown in Fig. 5, the toroidal magnetic field B_θ becomes from a diamagnetic to a paramagnetic profile in the closed flux region due to the

increase of u_z in the OFC region, while the diamagnetic B_θ profile is kept in the OFC region. The toroidal ion flow velocity u_θ is increased from negative to positive values in the closed flux region as shown in Fig. 5, enhancing the paramagnetic poloidal field. Here the negative u_θ is the opposite direction to the current. Both the poloidal and toroidal magnetic fields tend to become to the paramagnetic profiles, because both the poloidal and toroidal ion flow velocities tend to contribute to the plasma currents. The M-CHI effect leads the increase of plasma currents and magnetic flux.

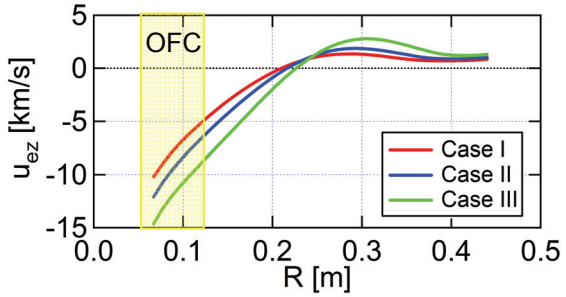

Fig.1 Radial profiles of the poloidal electron flow velocity u_{ez} at the midplane

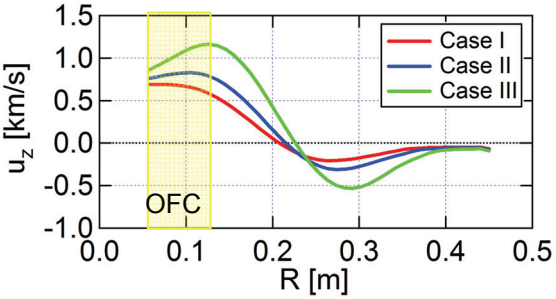

Fig.2 Radial profiles of the poloidal ion flow velocity u_z at the midplane

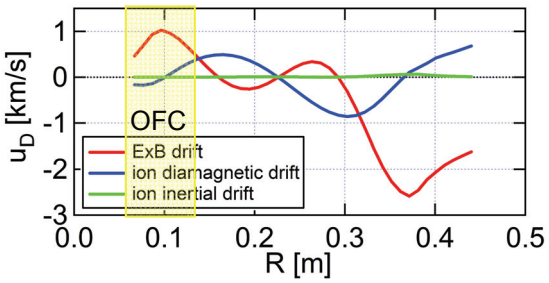

Fig.3 Radial profiles of the ion drift velocity u_D in the poloidal direction at the midplane in the case III

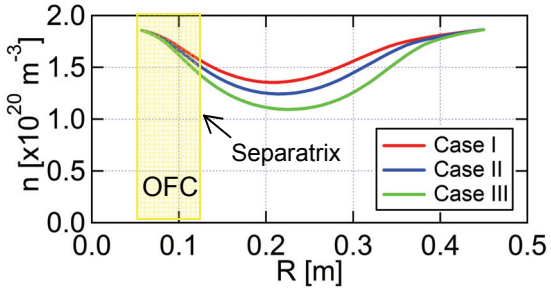

Fig.4 Radial profiles of the number density n at the midplane

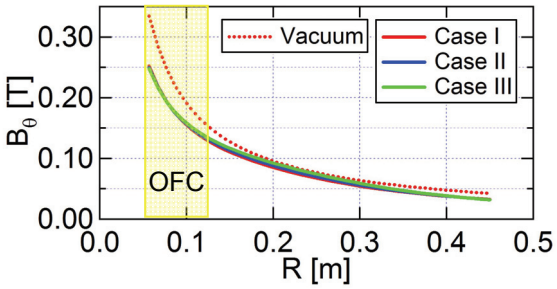

Fig.5 Radial profiles of the toroidal magnetic field B_θ at the midplane

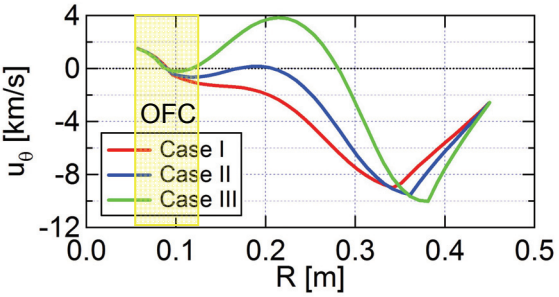

Fig.6 Radial profiles of the toroidal ion flow velocity u_θ at the midplane

References

[1] E.B. Hooper, Plasma Phys. Control. Fusion **53**, 085008 (2011).

[2] M. Nagata *et al.*, *24th IAEA Fusion Energy Conference* (San Diego, USA) ICC/1-1Rb (2012).

[3] L.C. Steinhauer and A. Ishida, Phys. Plasmas **13**, 052513 (2006).

[4] T. Kanki *et al.*, Plasma and Fusion Res. **3**, S1066 (2008).